2008 IEEE International Conference on
Robotics and Automation
Pasadena, CA, USA, May 19-23, 2008

An Explicit Model to Predict and Interpret Constraint Force Creation in pHRI with Exoskeletons

Andre Schiele

Abstract—**It is the goal of this paper to introduce an analytical model that allows predicting and interpreting the characteristics of constraint forces generated by misaligned joint axes between human operators and wearable robots during physical human-robot interaction (pHRI). The pHRI model is based on geometric parameters that describe the combined human-robot system. It is applied in this paper to measured constraint forces from a pHRI experiment. The model is validated with the experimental data.**

The geometrical model parameters are identified from force and position measurements by non-linear parameter optimization. The attachment stiffness and the actual offsets between the exoskeleton and the human joints are estimated. For the tested subject, the stiffness reaches 222 N/m and constraint forces are shown to be in the order of ± 10 N. It is shown in this paper how an ergonomically designed wearable robot with passive compensation joints can reduce such interaction forces.

I. Introduction

ROBOTIC exoskeletons are currently being developed in many research lab's for the rehabilitation of patients suffering from injuries to the nervous system. A multitude of exoskeletons for interaction with the human limb are proposed for rehabilitation training, ranging from external, end-point based devices to wearable full limb exoskeletons [1]. Their ability to smoothly interact with the human subject is crucial for successful application in physical therapy. It is important that devices interacting closely with a human limb are intrinsically safe, comfortable and are able to exploit the full range of natural motion for movement training. The two main aspects that need good consideration are the implementation of the actuation and motor control, as well as the intrinsic mechanical and kinematic design of their structure.

Still a couple of years ago, such rehabilitation exoskeletons were mostly equipped with motor controllers that dictated movement to the patient. While this seemed to suffice during the childhood of such devices, now, researchers want more freedom to implement assistive therapy protocols as well. In patient assist therapies, the robots actuation supports, but does not impose, the natural movement of the patient during training. Sophisticated controller concepts based on impedance control [2] are currently being implemented in such rehabilitation devices. Hybrid controllers in rehabilitation exoskeletons provide significantly better safety for the user than the earlier position controllers. Thus, from an actuation and motor control point of view, safety and user comfort criteria can be satisfied for wearable robots, or at least will be soon.

An area, however, to which too little attention is paid, is the appropriate kinematic design of wearable robot structures. If the kinematic setting of an exoskeleton robot is not well matched to the user, undesired interaction forces can be created during motion, even if no actuation is provided at all. Those constraint forces could be large in magnitude and provide a safety hazard as well as discomfort to the user. It is interesting to note that such forces, stemming mostly from misalignments between the device's axis of motion and the human limb, can usually not be compensated by the device's actuators. Kinematic mismatches between the Lokomat leg orthosis and patient legs, for instance, were already shown to be responsible for injuries and discomfort. This was reported in [3] and [4]. Furthermore, it was shown in [5] that kinematic mismatch between an orthosis and a patient can alter the natural muscle activation patterns. This is counterproductive during physical therapy and could also lead to injury.

Based on such observations, in 2006, we have developed a novel design paradigm for better mechanical and kinematic exoskeleton designs. The paradigm was presented in [6] on the example of the ESA ergonomic human arm exoskeleton. Currently we are performing an extensive experiment study to analyze the differences between ergonomic and non-ergonomic exoskeleton designs in terms of user comfort and task performance. One element that we measure during this campaign is the constraint forces in a variety of device settings along with their characteristic over the movement angle of the limbs. Looking at the first graphs we immediately noticed that a model will be required to interpret the characteristics of the forces measured. Fitting a general model does not yield the relation between the measured data and the physical model parameters. Therefore an explicit model is required.

It is the goal of this paper to establish and validate an explicit analytical model suitable to predict and interpret constraint forces between human operators and robots during physical human-robot interaction (pHRI). This paper will moreover show how the model can be used to determine center of rotation offsets and the attachment stiffness in the combined human-robot system, from measured data.

Manuscript received September 14, 2007.

A. Schiele is with the Mechanical Engineering Department of the European Space Agency, Automation & Robotics Section, Noordwijk, 2201 AZ (phone: +31 71565 3760; fax: +31 71565 5419; e-mail: Andre.Schiele@esa.int).

II. pHRI Model

A. Approach

A mechanical model can describe the causes and effects of centre of rotation offsets between a human joint and a wearable robot joint. Such offsets create displacements of the robots attachment points along the human limb during joint motion. Those displacements will cause forces on the operator limbs.

For simplicity, a one degree of freedom model of human and robotic joint motion will be presented in this paper. The model is illustrated for the elbow joint, but is equally applicable to all other single degree of freedom joints of the human body that can interact with a wearable robot. The model will also be used to estimate unknown experimental parameters such as offsets and attachment stiffness from a real pHRI experiment. A model verification will be performed with a set of experiment data.

Once the model is proven suitable to explain apparent forces in terms of the physical model parameters, it will provide invaluable help in analyzing the effects of wearable robot design to operator comfort.

B. Mechanical Model for Single D.o.F. pHRI

A combined physical human-robot interaction system can be simplified as illustrated in Fig. 1. A human operator wears an exoskeleton that is attached at two locations on his limbs. In the example shown, those two locations are the upper-arm and the forearm respectively. On the left illustration in the figure, the estimated kinematic structure of a human limb is shown in light grey colored lines. The estimated, but unknown position of the true human elbow rotation axis, or instantaneous centre of rotation (ICR_h) is indicated with a grey dot and black cross. The exoskeleton structure is schematically shown as well. Its elbow joint centre of rotation (CR_e) does not align well to the operator elbow. For this explicit model, a rigid fixation of the exoskeleton on the upper arm is assumed. A soft, more compliant fixation is assigned to the forearm fixation.

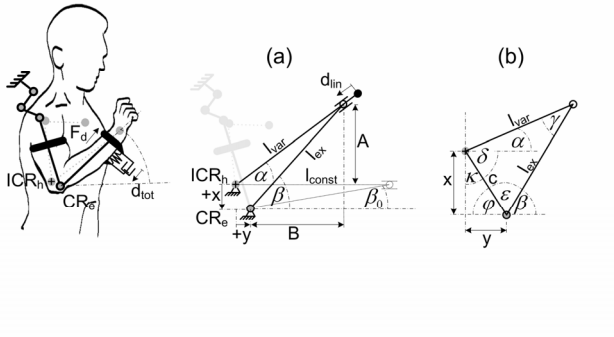

Fig. 1. Mechanical model of single degree of freedom interaction between a human joint and a wearable robot. The model is used to predict the constraint displacements d_{tot} that exist between the limb and the robot if their centre of rotations (ICR_h, CR_e) have offsets (x,y).

The soft fixation can be modeled for instance with a Voigt-element, that simulates viscoelastic properties. The element-parameters would then describe the lumped viscoelastic properties of the entire coupling between the rigid human forearm and the rigid exoskeleton mechanism. Thus, including muscles, soft tissues, the skin as well as the soft attachment pads of the exoskeleton. It is important to notice, that also the upper-arm fixation will have an influence on the interaction displacements and forces created between the robot and the human limb. For sake of simplicity, however, this will be neglected in this model. The sketch in Fig. 1 (a) abstracts the pHRI of this situation into a static mechanical problem. Any offset x or y between the ICR_h and the CR_e will create a constraint displacement d_{tot} of the distal exoskeleton fixture along the forearm of the operator. Through the soft coupling between human and robot, a force F_d will be created according to

$$F_d = k \cdot d_{tot}\left(\beta, x, y, l_{ex}, z_{ex}\right) + b \cdot \dot{d}_{tot}\left(\dot{\beta}, x, y, l_{ex}, z_{ex}\right) \qquad (1)$$

In this simplified case, d_{tot} is a function of the elbow exoskeleton rotation angle β. The offsets x, y as well as the design parameters l_{ex} (link length) and z_{ex} (link offset) of the exoskeleton, are the parameters characterizing the constraint force. In (1), k denotes the lumped stiffness and b the lumped velocity dependent damping of the coupling between wearable robot and the human bone. In order to understand the magnitudes and behaviour of the constraint force, it is most important to first derive the magnitudes and characteristics of the constraint displacement d_{tot} in dependence of the robot parameters and offsets. This allows us to establish an explicit kinematic model.

The displacement d_{tot} has a linear (d_{lin}) and a rotary (d_{rot}) component. Let us first concentrate on the linear component d_{lin} depicted in Fig. 1 (a). For the purpose of this paper, all equations will be derived in dependence of the angle β. They could be derived for α but β can be directly measured on the exoskeleton and thus the measured data can be used as input to the parameter identification later on. It is more difficult to measure the human rotation angle α during an experiment. The angles α and β are geometrically related, however, as we shall see. In order to establish $d_{lin}(\beta)$, from Fig. 1 we determine the relationship

$$d_{lin}\left(\beta\right) = l_{const} - l_{var} \cdot \qquad (2)$$

With,

$$l_{const} = y + \cos\left(\beta_0\right) \cdot l_{ex} \; ; \beta_0 = \sin^{-1}\left(x / l_{ex}\right)$$

$$l_{const} = y + l_{ex} \cdot \sqrt{1 - \left({x^2} \Big/ {l_{ex}}^2 \right)} \; . \qquad (3)$$

The parameter l_{const} describes the distance between the distal attachment of the exoskeleton and the limb rotation axis if the flexion is zero.

Now, only l_{var} remains to be determined. From Fig. 1 (a), l_{var} can be expressed as

$$l_{var} = \sqrt{(B+y)^2 + A^2} \; ; A = \tan(\alpha)\cdot(B+y),$$
$$B = \cos(\beta)\cdot l_{ex} . \quad (4)$$

Consequently,

$$l_{var} = \sqrt{(y + l_{ex}\cdot\cos(\beta))^2 \cdot \sec(\alpha)^2} . \quad (5)$$

Equation (5) allows expressing d_{lin} in dependence of either α, β or both. Deriving for α will not be further performed in this paper. In order to express d_{lin} only in dependence of β, we must derive the relationship $\alpha(\beta)$ between the two angles. The relationship between α and β is to be purely dependent on the geometric conditions l_{ex}, x and y. Refer to Fig. 1 (b) for the following assumption

$$\delta + \gamma + \varepsilon = \pi . \quad (6)$$

With,

$$\delta = \pi - ((\pi/2) - \alpha) - \kappa \; ; \kappa = \tan^{-1}(y/x), \quad (7)$$

and

$$\varepsilon = \pi - \varphi - \beta \; ; \varphi = \tan^{-1}(x/y), \quad (8)$$

follows the relationship between α, γ and β

$$\alpha = -\gamma + \beta . \quad (9)$$

Under consideration of the property

$$\pi/2 = \tan^{-1}(y/x) + \tan^{-1}(x/y). \quad (10)$$

In order to derive $\alpha(\beta,x,y,l_{ex})$ from (9), we must express γ also as a function of β and the geometric conditions. It can be seen in Fig. 1 (b) that the height on the side l_{var} of the triangle equals

$$c\cdot\sin(\varepsilon) = l_{var}\cdot\sin(\gamma). \quad (11)$$

With the general law of cosines we can express l_{var} alternatively as

$$l_{var} = \sqrt{c^2 + {l_{ex}}^2 - 2\cdot c\cdot l_{ex}\cdot\cos(\varepsilon)} \; , \; c = \sqrt{x^2+y^2} . \quad (12)$$

Thus, substituting (12) with (8) into (11), and solving for γ yields after simplification:

$$\gamma(\beta) = \sin^{-1}\left(\frac{\sqrt{x^2+y^2}\cdot\sin\left(\beta + \tan^{-1}\left(x/y\right)\right)}{\sqrt{{l_{ex}}^2 + x^2 + y^2 + 2\cdot l_{ex}\cdot\sqrt{x^2+y^2}\cdot\cos\left(\beta+\tan^{-1}\left(x/y\right)\right)}} \right) \quad (14)$$

It is worth mentioning here that γ creates also a rotary displacement of the attachment cuff on the forearm. We will therefore come back to γ when we discuss the contribution of d_{rot} to d_{tot}. Now, $\alpha(\beta,x,y,lex)$ can be easily derived by factoring (14) into (9). The linear displacement d_{lin} is then determined by inserting $\alpha(\beta,x,y,lex)$ into (5), and then into (2).

After simplification we get

$$d_{lin}(\beta) = l_{ex}\cdot\sqrt{1 - \frac{x^2}{{l_{ex}}^2}} + y$$
$$- \sqrt{\left(y + l_{ex}\cdot\cos(\beta)\right)^2 \cdot \csc\left(\beta + \cos^{-1}\left(\frac{c\cdot\sin\left(\beta+\tan^{-1}\left(x/y\right)\right)}{\nabla}\right)\right)} \; ;$$

$$\nabla = \sqrt{{l_{ex}}^2 + x^2 + y^2 + 2\cdot l_{ex}\cdot c\cdot\cos\left(\beta + \tan^{-1}\left(x/y\right)\right)} . \quad (16)$$

Equation (16) describes the linear displacement of a wearable robot of a structure shown as in Fig. 1. Often, however, a wearable robot features an additional link offset z_{ex} around its distal attachment point, similar than depicted in Fig. 2. If such an offset exists, the rotation introduced by γ will alter the total constraint displacement d_{tot} with an error contribution d_{rot} according to

$$d_{rot} = \tan(\gamma)\cdot z_{ex} . \quad (17)$$

The total constraint displacement d_{tot} therefore can be calculated by

$$d_{tot}(\beta,x,y,l_{ex},z_{ex}) = d_{lin} - d_{rot} . \quad (18)$$

With d_{tot} known, the interaction force F_d can be estimated by (1) if the stiffness and damping constants are known.

III. pHRI Model Identification

A. Goal

The model will be crucial to assign specific force characteristics over the range of motion to the geometric parameters at stake. Without it, no explanation could be offered about the characteristic shapes of forces over workspace.

Mostly, the offsets between a wearable robot joint and a human limb are not known in practice. Equally, the stiffness and damping parameters of the attachments are hardly known for the current experimental setting. It is not practical to measure the parameters x, y, l_{ex}, z_{ex}, k and b directly. We use the model presented before to identify those parameters from experimentally measured force and position data.

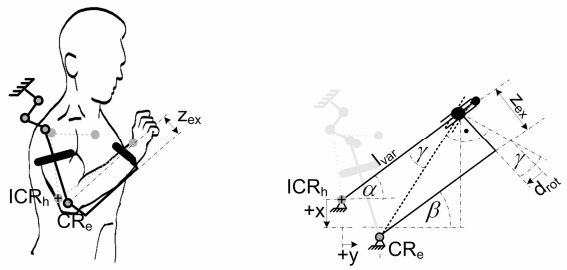

Fig. 2. If the wearable robot features mechanical offsets z_{ex}, a further constraint displacement d_{rot} is introduced that can create torques around the attachment point.

Currently ESA is carrying out an experimental investigation aiming at deriving the influence of interaction forces created by ergonomic and non-ergonomic designed wearable robot interfaces on operator comfort and task performance during pHRI. In the course of those experiments, interaction force is measured between test persons and wearable robots during execution of a set of tracking tasks. In this paper, the data of one subject was used for the verification of the pHRI interaction model presented above.

It is the goal of this identification to derive the geometric parameters x, y, l_{ex}, z_{ex} as well as the attachment stiffness k from measured data. This allows proofing suitability of the model to help in the interpretation of the results.

B. Experiment Method

The subject conducted the following experiment with the ESA human arm exoskeleton. The EXARM exoskeleton is an ergonomic device, as presented in [6] [7] [8]. It features passive joints which shall compensate for any misalignments between the human and exoskeleton centers of rotation. Therefore, the EXARM, in this setting, is supposed to not create large interaction forces F_d during motion. In this experiment, the subject performed 12 tracking tasks. For 6 tasks the exoskeletons passive compensatory joints were locked, to emulate a conventional, non-ergonomic robot. For the other 6 tasks, the compensatory joints were free to move. We call this setting the "unlocked" setting. In both settings, the attachment pressure of the device on the limb was randomized between 10 – 60 mmHg. The "unlocked" and "locked" settings were randomized as well. Before each task, the exoskeleton was dressed to the subject to approximately match the CR_e to the ICR_h. The test person had a statue of 1.71 m and a body mass of 63.0 kg.

Once the device was dressed on, the test person was asked to track a multisine position signal on a computer screen with his elbow movement. The elbow movement was also displayed on the screen. All forces between the human forearm and the exoskeleton were measured with a 6 DOF Force and Torque Sensor (ATI, Nano Series) integrated in the exoskeleton mechanical structure. The tracking signal contained a range of varying random frequencies from 0.05 to 0.35 Hz and amplitudes from 0 to Pi. Each experiment run had a duration of 60 s and data was acquired every 1 ms. The test person wearing the exoskeleton is shown in Fig. 3.

C. Experiment Data

For the purpose of the parameter identification and pHRI model verification, data collected during the "locked", non-ergonomic experiment runs are used. All compensation joints of the exoskeleton were locked. The data from the "unlocked" runs is used to show the motion of the exoskeletons linear compensation joint that should match the displacement d_{tot}. Data acquired during all experiments is the rotation angle β of the exoskeleton and the force F_d along the axis of the forearm (direction corresponding to Fig. 1).

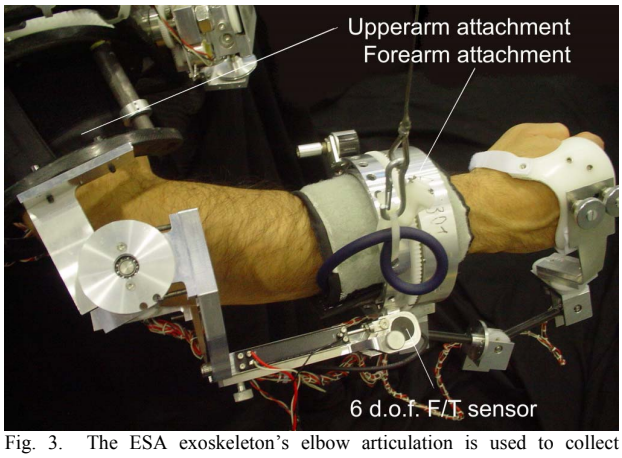

Fig. 3. The ESA exoskeleton's elbow articulation is used to collect measurement data of interaction forces F_d and constraint displacements d_{tot}.

The rotation angle is measured by a precision potentiometer on the exoskeleton. For the "unlocked" setting, also the displacement d_{tot} (that takes then place in the, free-to-move linear compensation joint) is measured directly by a precision potentiometer. All signals were filtered analog to reduce noise to less than the quantization level (12 bit).

In order to investigate the forces over the entire range of joint motion, the data was binned for processing. Depending on the desired output, angle bins of 2 degrees ranging from 0 – Pi were used (42 bins). For some illustration purposes, larger bins were produced in 10 degree steps of β.

The mechanical linkages of the exoskeleton have the following geometric parameters. The forearm linkage length l_{ex} ranges from 0.16 – 0.21 m and the distal offset z_{ex} ranges from 0.06 – 0.13 m, depending on the actual contact point of the arm inside the fixation cushion.

D. Identification Procedure

The identification aims at finding suitable model parameters $\vec{\varepsilon}$ for the pHRI model to optimally match the experimental data (F_{di}, β_i). The pHRI model presented above is non-linear in its parameters, which is why we chose to formulate the identification as a non-linear optimization problem in the least squares sense. The parameters were identified by minimizing

$$Q(\vec{\varepsilon}) = \sum_{i=1}^{42} \left[F_{d_i} - k \cdot d_{tot}(\beta_i, \vec{\varepsilon}) \right]^2 \quad \vec{\varepsilon} = \left(\hat{x}_i, \hat{y}_i, \hat{l}_{exi}, \hat{z}_{exi} \right). \tag{19}$$

A linear relationship between displacement and force was taken as a first assumption for the validation in this paper. Velocity dependent effects were not considered.

The optimization was solved numerically using an implementation of the Levenberg-Marquardt algorithm. Initial guesses of the parameters were based on experience, visual analysis of the center of rotation offsets and the geometric design data of the EXARM exoskeleton.

Also, manual manipulations with the model parameters where performed to find the correct behavior of the constraint force over the motion range. The starting guesses of the search were k = 300 N/m, x = 0.03 m, y = 0.04 m, l_{ex} = 0.2 m, z_{ex} = 0.12 m. The upper and lower bounds for searching l_{ex} and z_{ex} were set to the range of possible values for the given EXARM mechanical design.

To quantify how good the model matches the measured data, we used a variety of measures. First, the coefficient of determination R^2 was used to analyze the proportion of variability in the measured data that is accounted for by the model. R^2 was determined according to

$$R^2 = \left(\sum_{i=1}^{n} (F_{di} - \bar{F}_{di})^2 - \sum_{i=1}^{n} \left(F_{di} - \hat{k} \cdot \hat{d}_{tot} \right)^2 \right) / \sum_{i=1}^{n} \left((F_{di} - \bar{F}_{di})^2 \right). \quad (20)$$

Next, we performed a graphical analysis of the residuals, to check whether the model structure represents the measured data well. The graphical analysis of the residuals included plotting the residuals over the angle β to check whether they are randomly distributed. A second plot, showing a histogram of the residuals was performed to check for normal distribution of the residuals. Normal distribution of the residuals was then checked by the Lilliefors adoption of the Kolmogorov-Smirnov test.

IV. Results

A. Measurements of Constraint Force F_d during Experiments

The resulting constraint forces during motion of the elbow articulation with the exoskeleton are shown in Fig. 4 plotted over the exoskeleton elbow rotation angle β. In Fig. 4 (a), the results for the "locked" settings of the exoskeleton are depicted, whereas Fig. 4 (b) depicts the interaction forces that were present during the trials with the "unlocked" setting. Boxplots respectively show the accumulated F_d measurements for 6 experiment tasks of 60 s each (at 1 kHz sampling). It can be seen that the constraint forces range from about -13.5 N – 10 N for the conventional "locked" setting, while for the "unlocked" setting they range only from about -6 N – 2.6 N. For both cases, the force bins are significantly different ($p<0.01$) from one angle bin to another. Thus, there is a clear trend apparent in the data.

B. Model Outputs for Constraint Displacements d_{tot}

Predictions of the constraint displacement d_{tot} from the model established above are depicted in Fig. 5. Whereas the surface plot shown in Fig. 5 (a) depicts displacements exclusively induced by offsets in x direction, Fig. 5 (b) depicts the displacements as a function of offsets in the y direction only.

For both plots, l_{ex} was set to 0.2 m while z_{ex} was set to 0.08 m. It can easily be seen that the behavior of the displacements is complex and very dependent on the offsets. The graphs show that individual misalignments create displacements that are not negligible. A pure y displacement of 10 cm for instance, can create a displacement of a wearable robot along the forearm of about 15 cm during total flexion of the elbow (corresponding to β ~ ¾ Pi).

C. Model Identification with "Locked" Data Set

1) Resulting model parameters: The measured data presented in Fig. 4 (a) was used as input to the optimization algorithm. However, a finer discretization of the angle bins was performed and the mean value of the constraint force F_d in each angle bin was used as actual input. The mean values are depicted in Fig. 6 by black dots over the exoskeleton elbow joint angle. The optimal parameters that the algorithm converged to are:

$$k = 222.43 \text{ N/m}, x = 0.048 \text{ m}, y = 0.059 \text{ m}$$
$$l_{ex} = 0.169 \text{ m}, z_{ex} = 0.127 \text{ m}.$$

The estimated model with the above parameters is displayed as a solid line in Fig. 6. Note that towards $\beta = 0$, no data exists. This is the case, because the test person did not reach the 0 degree stroke end with the exoskeleton in the setting with the compensation joints locked.

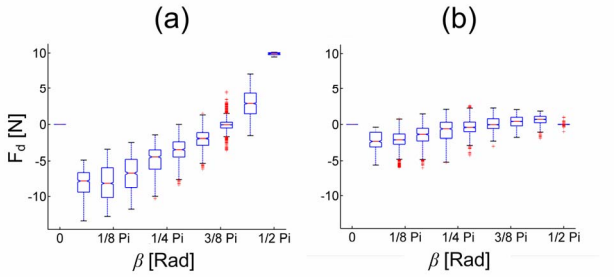

Fig. 4. Measured constraint forces F_d along the axis of the test subjects forearm. Boxplots show the characteristics of those forces for (a) non-ergonomic exoskeleton settings without passive joints ("locked") and (b) ergonomic exoskeleton setting with compensation joints ("unlocked"), over 10 different elbow rotation angles β.

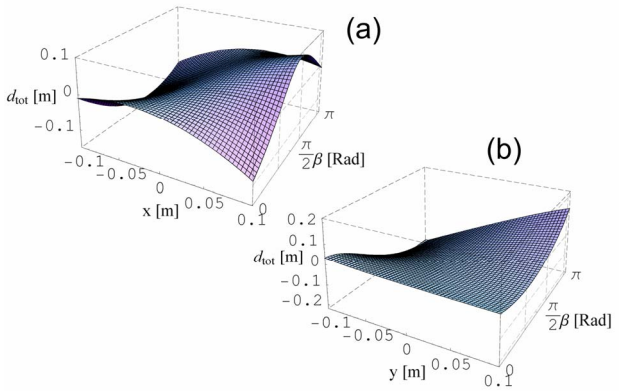

Fig. 5. Predicted constraint displacements d_{tot} [m] in dependence of the offsets x and y between the human limb rotation axis ICR_h and the exoskeleton rotation axis CR_e. In (a) the model output is shown for variable x offsets with y equal to zero. In (b) the model output is shown for variable y offsets with x equal to zero.

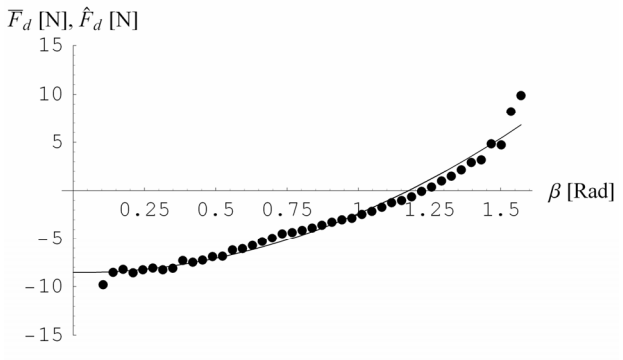

Fig. 6. Means of all measured interaction forces F_d during "locked" trials over the exoskeleton elbow angle (points). The result of the estimated interaction force F_d with identified parameters x, y, l_{ex} and z_{ex} of the pHRI model is shown by the superimposed line.

2) Model validation: The coefficient of determination R^2 shows that the regression line approximates the real data points well (R^2 = 0.973). The coefficient was determined with a different data set then the original input data to the model. This alone, however, does not confirm that the underlying model is suitable. Fig. 7 depicts the graphical residual analysis. In Fig. 7 (a), the residuals are plotted over the input angle β. The residuals are spread around 0 and seem to be equally present in the positive and negative half of the plot. However, the residual might reveal a still underlying trend of the data. Therefore Fig. 7 (b) was created that depicts a histogram of the residuals. The residuals are centered around a mean of -0.006 N, with the median at -0.033 N and standard deviation of ± 0.782 N. Two outliers are visible close to the data minimum of -3.088 N. The Lillieforts test showed that the residuals are normally distributed ($p<0.05$).

D. Constraint Force Difference in "Unlocked" and "Locked" Exoskeleton Setting

The measured constraint forces F_d are shown for both settings, "locked" (dots) and "unlocked" (circles) in Fig. 8. All data presented there is averaged over 6 trials and binned into 2 Deg. narrow angle bins. The measured displacement d_{tot} of the compensatory exoskeleton joint is shown (crosses).

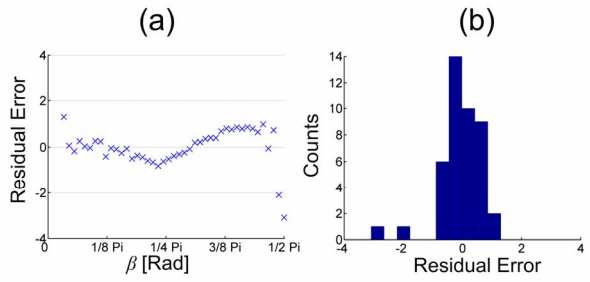

Fig. 7. In (a) a plot of the residual errors between the measured data and model estimates show good distribution around 0. In (b), the histogram indicates a normal distribution of the fitting residuals. This indicates that the model structure is suitable for interpreting the measured data.

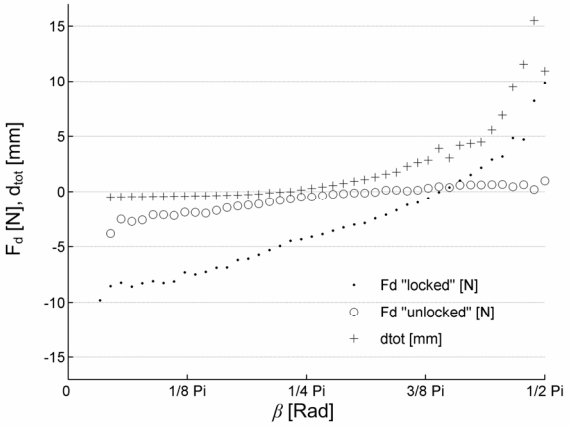

Fig. 8. The measured constraint forces F_d are shown for both exoskeleton settings, "unlocked" (compensation joints free to move) and "locked" (compensation joints fixed). The measured displacement of the exoskeleton compensation joint during "unlocked" trials is superimposed. This shows that the setting with passive compensation joints yields lower interaction forces for the test subject.

The displacement was acquired during the trials with the compensation joint of the exoskeleton free.In the other trials this value is constantly zero because the joint is locked. It can be seen that in the "unlocked" setting of the wearable robot, the force F_d approximates null, when the compensatory joint starts displacing. In contrast, during the "locked" trials, the force builds up during larger angles.

V. Discussion

From Fig. 4 it can be seen that the characteristics of the constraint forces are intrinsically different for the assumed ergonomic setting, in which passive exoskeleton joints are present and the "locked" setting, for which the passive joints have been locked. Also, when looking at the characteristic of the trend, it is not apparent why a constraint force exists close to $\beta = 0$. Our established model is now instrumental to find out which geometric parameters are responsible for this characteristic. The negative force F_d at $\beta \sim 0$ is attributed in this case to a combination of offsets of the centers of rotation in $+x$ and $+y$ direction. This was revealed from the model identification performed above. (See Fig. 6) From manually altering some of the parameters of the model we learned furthermore that the offset z_{ex} plays a crucial role in the large negative forces at small β angles. If z_{ex} is zero, the force offsets at small angles β converge towards zero as well. It can be seen in (17) that then d_{rot} converges to zero, which is the cause. In Fig. 4 (b), the initial offset is smaller. This is due to the fact, that the exoskeleton has also a passive rotary joint that was free to move in this condition. The rotary joint removes a large share of the influence of z_{ex} on the force. A main difference between the force trends shown in Fig. 4 (a) and Fig. 4 (b) is also the fact that one force rises after crossing from negative to positive (a) and the other levels off after approaching null from below.

This can be explained under the consideration of Fig. 8. A negative force F_d pushes the distal attachment of the wearable robot toward the proximal direction (See the sign convention in Fig. 1 for reference). We can see in Fig. 8 that also in the "unlocked" setting of the exoskeleton, a negative constraint force exists up to an elbow rotation angle of about 55 Deg. This was unexpected. At the same time, there is no excursion of the linear compensation joint that is normally free to move in this exoskeleton configuration. By knowing the meaning of a negative force F_d through our model, we can explain the situation. Logically, this must mean that the negative stroke end of that linear compensation joint is still too large for this test person. The linear joint starts moving only, after the force levels off. For the kinematic design of the exoskeleton this means that the minimum of the passive joint stroke end must be further decreased. Then, the negative force component, that could be felt as disturbance can be reduced.

This way, our model allows drawing direct conclusions about improving the ergonomic exoskeleton design. In the conventional setting, depicted in Fig. 8 by the black dots, we see that the locking of the passive compensatory joint creates a positive constraint force along the direction of the forearm for elbow rotations larger then about 67 Deg. There, the force is not cancelled out by the passive joint movement.

The performed parameter identification of the model shows that an attachment stiffness of about 222 N/m exists between the human and the wearable robot. By using this identification technique, we will be able to determine relations between attachment stiffness and comfort of the operators in future experiments. The identified parameters of l_{ex} and z_{ex} make physically sense. They lie perfectly within the possible ranges dictated by the mechanical exoskeleton design. Given those geometric distances, we can determine the exact location of the contact point between the human arm and the exoskeleton. This, in turn, helps to identify the precise torque that can be transferred from attached actuators to the human joint.

The scatter plot of the fit residuals shown in Fig. 7 shows a roughly equal distribution of the residuals around 0, which is a good sign for a model fit. Also, the residuals are normally distributed. In general, we can conclude that the model is sufficiently well in structure, to explain the trends of the measured data.

The parameter identification procedure has revealed the precise offsets between the human and exoskeleton joint, which, without the model, would have stayed a mystery.

VI. Future Work

In an ongoing experiment campaign, we will investigate with more subjects, what the influence of constraint forces is on task performance, user comfort and mental load. The established and validated model will help to assign subjective and objective performance measures to geometric conditions of the human-robot interaction. The model has already revealed some possible improvements to the EXARM exoskeletons kinematic structure. For the second prototype, that we are currently building, the passive compensatory joint design will be adapted accordingly. Furthermore, the novel prototype shall not contain an offset z_{ex} that contributes significantly to creation of constraint forces even at small limb flexion angles.

VII. Conclusion

(1) An analytical model for predicting and analyzing constraint force in pHRI has been proposed and validated with experimental data. (2) The pHRI model is suitable to relate measured characteristics of constraint forces to geometric conditions of a combined human-robot system. The model therefore provides crucial insights into pHRI that otherwise can not be explained. (3) By identifying the physically meaningful parameters of the model, shortcomings in our current exoskeleton design have been discovered. (4) For one experiment subject it was shown that the EXARM exoskeleton with passive compensation joints yields significantly smaller interaction forces than an exoskeleton without such joints.

References

[1] R. Riener, T. Nef, G. Colombo, "Robot-aided neurorehabilitation of the upper extremities", Med. Biol. Eng. Comput., 43, pp.2-10., 2005.

[2] N. Hogan, "Impedance control: An Approach to Manipulation, Parts I, II, III,", Journal of Dynamic Systems, Measurement, and Control, vol. 107, pp. 1-23, 1985

[3] G. Colombo, M. Joerg, V. Diez, "Driven Gait Orthosis to do Locomotor Training of Paraplegic Patients", Proc. 22nd Annual EMBS Conf., Chicago, July 23-28,2000.

[4] G. Colombo, M. Joerg, R. Schreier, V. Dietz, "Treadmill training of paraplegic patients using a robotic orthosis", Journal of Rehabilitation Research and Development, Vol. 37., No.6, pp. 693 - 700, Nov/Dec., 2000.

[5] J. M. Hidler, A.E. Wall, "Alterations in muscle activation patterns during robotic-assisted walking", Clinical Biomechanics 20, pp184 – 193, 2005.

[6] Schiele A., van der Helm F.C., "Kinematic design to improve ergonomics in human machine interaction", IEEE Trans Neural Syst Rehabil Eng, Dec., 14(4), 456-69, 2006

[7] A. Schiele, M. De Bartolomei, F.C.T. van der Helm, "Towards Intuitive Control of Space Robots: A Ground Development Facility with Exoskeleton", In Proc. Of IEEE/RSJ Int. Conference on Intelligent Robots and Systems, 2006, pp. 1396 – 1401

[8] A. Schiele et al., Bowden Cable Actuator for Force-Feedback Exoskeletons, In Proc. Of IEEE/RSJ Int. Conference on Intelligent Robots and Systems, 2006, pp. 3599 – 3604